Optics Letters

Soliton-mediated orientational ordering of gold nanorods and birefringence in plasmonic suspensions

Yu-Xuan Ren,[1] Trevor S. Kelly,[1] Chensong Zhang,[1] Huizhong Xu,[1] and Zhigang Chen[1,2,*]

[1]Department of Physics and Astronomy, San Francisco State University, San Francisco, California 94132, USA
[2]TEDA Applied Physics Institute and School of Physics, Nankai University, Tianjin 300457, China
*Corresponding author: zhigang@sfsu.edu

Received 30 November 2016; revised 4 January 2017; accepted 5 January 2017; posted 11 January 2017 (Doc. ID 281862); published 1 February 2017

We report on the soliton-mediated orientational ordering of gold nanorods in a colloidal plasmonic suspension. Due to the nonlinear optical response of the suspension, a light beam forms an optical spatial soliton which creates an effective optical waveguide. The orientation of the nanorods along the waveguide is regulated by the optical torque exerted by the linearly polarized soliton beam. By measuring the polarization transmission spectrum of a probe beam at a wavelength far from the plasmonic resonance, we observe orientation-enhanced birefringence along the soliton channel, suggesting a disorder-to-order transition of nanorods due to the action of the soliton beam. This approach may be applied in other colloidal systems with optical force-induced nonlinearity.

OCIS codes: (190.6135) Spatial solitons; (250.5403) Plasmonics; (160.4330) Nonlinear optical materials; (190.3970) Microparticle nonlinear optics.

https://doi.org/10.1364/OL.42.000627

Metallic nanoparticles have widespread applications due to the tunability of their optical, plasmonic, and photothermal properties [1–3]. The plasmonic resonance of the nanorods can be controlled by tuning their size and shape, resulting in different responses to light frequency, polarization, and momentum [2,4]. In optical trapping experiments, it has been demonstrated that an optical beam with angular momentum can rotate either birefringent or absorbing particles [5–7], and that an optical wrench produced by circularly polarized light can allow for the detection of the torque on a DNA tethered to the birefringent particle [6]. Even a linearly polarized beam is sufficient to optically align anisotropic particles due to the anisotropic polarizability [5]. In particular, both the optical trapping and the fluorescence correlation spectroscopy experiments have revealed that a single plasmonic nanorod trapped with a near-infrared (IR) laser tends to reconfigure itself to orient with the light polarization [8–10], apart from other experiments such as polarization-dependent white-light transmission spectrum [11]. A theoretical study with the Maxwell tensors also revealed that elongated gold nanorods tend to align themselves with the long axis parallel to the beam polarization when the wavelength of light is greater than that of the longitudinal surface plasmon resonance (LSPR) [12], but perpendicular to the polarization when the wavelength is smaller than that of the LSPR [12–14]. This orientation effect, originating from the optically induced torque, could bring about phase change and optical anisotropy for the nanorod ensembles [9,11,15,16].

Our previous studies have demonstrated that even an off-resonant laser beam could create a soliton channel in gold nanorod suspensions, thanks to the strong self-focusing nonlinearity originated from optical forces [4,17]. In this Letter, we demonstrate optical soliton-induced orientational ordering of nanorods in the gold nanoparticle suspensions. By sending a probe beam with varying linear polarization into the soliton channel, we measure the polarization transmission spectrum and compare with the cases when there is no soliton beam, or the soliton beam is circularly polarized. The polarization-dependent modulation in transmitted power, observed only when the soliton beam is linearly polarized, is attributed to birefringent absorption (difference in the imaginary part of the refractive index) as a result of soliton-induced reorientation of gold nanorods). Similar experiments with gold nanosphere suspensions led to soliton formation, but not the enhanced birefringence. The observed phenomenon is fundamentally different from those due to optically induced thermal effects or nonlinear effects in polymers and liquid crystals [18–20].

The physical picture for soliton-mediated orientational ordering is illustrated in Figs. 1(a) and 1(b). Naturally, the nanorod suspension is isotropic at room temperature, which implies that the nanorods are randomly oriented. Once the plasmonic soliton is established, the nanorods experience an optical potential and, thus, reorient with respect to the polarization of the soliton beam, and the rotational degree of freedom is highly suppressed. This configuration is triggered by the soliton-mediated optical torque on the nanorods. A rod can be modeled as a prolate spheroid with a long semi-axis a and two identical short semi-axes b ($a > b$). The prolate rod is polarized by an electromagnetic field,

with the frequency-dependent polarizabilities parallel (along long axis) and perpendicular (along short axis) to the polarization described by [11,21]

$$\alpha_{\parallel,\perp} = 4\pi ab^2\epsilon_m \frac{\epsilon_1 - \epsilon_m}{3\epsilon_m + 3L_{\parallel,\perp}(\epsilon_1 - \epsilon_m)}, \quad (1)$$

where ϵ_1 and ϵ_m are the frequency-dependent complex dielectric constants of gold and the surrounding medium. The geometrical structure factor along the longitudinal mode direction is

$$L_{\parallel} = \frac{1 - e^2}{e^2}\left(-1 + \frac{1}{2e}\ln\frac{1+e}{1-e}\right), \quad (2)$$

where the eccentricity e is defined as $e^2 = 1 - b^2/a^2$. The geometric factor along the short axis is $L_{\perp} = (1 - L_{\parallel})/2$. For simplicity, let us assume that the rod is initially aligned in the transverse plane [Fig. 1(d)]. Naturally, the orientations of nanorods in the suspension are random, resulting in an isotropic phase and, thus, the ensemble average of the orientation angle $\langle\beta\rangle = 0$, where β represents the angle of the director (long axis) with respect to the polarization direction of the soliton beam. From Eq. (1) and theoretical calculation [4], it can be determined that the polarizability of gold nanorods at 532 nm wavelength is negative along the long axis, but positive along the short axis [Fig. 1(c)]. Thus, those rods with the long axis aligned in parallel with the beam polarization will be repelled, while those with the long axis perpendicular to the beam polarization will be attracted by the soliton beam [22,23]. For those rods that are initially oriented in other arbitrary directions, the optical torque will rotate them so their long axes can be aligned to the perpendicular direction.

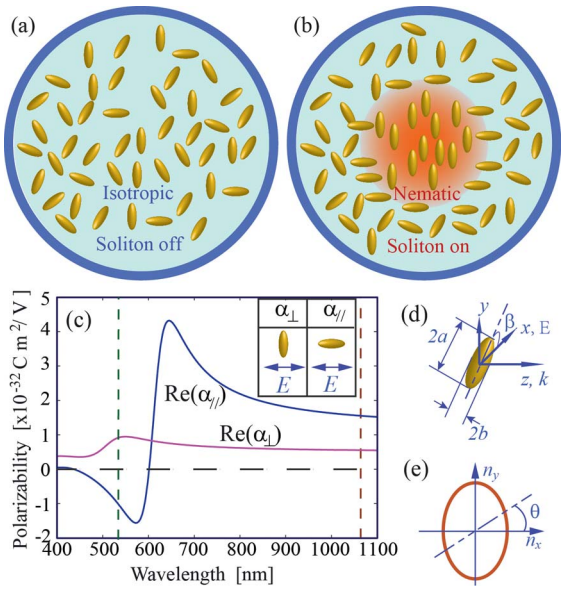

Fig. 1. (a) Gold nanorods naturally assume random orientations in the aqueous solution (isotropic phase). (b) Soliton beam rotates nanorods and aligns their long axes toward the direction perpendicular to the laser polarization (nematic phase) due to optical torque from the soliton beam. (c) Parallel and perpendicular polarizabilities of a single nanorod as a function of the laser wavelength, showing opposite polarizabilities at 532 nm (marked by left dashed line). The right dashed line marks the probe beam wavelength at 1064 nm. (d) Schematic of the rod orientation with β being the angle between the long axis of the nanorod and the polarization of the soliton beam (the x-axis). (e) Illustration of refractive indices in the orthogonal directions due to induced optical anisotropy. The dashed line shows the polarization direction (angle θ) of the incident probe beam.

In theory, the misalignment between the induced dipole moment of a nanorod $\boldsymbol{P}$ and the optical field $\boldsymbol{E}$ results in a torque $\tau = \boldsymbol{P} \times \boldsymbol{E}$, which is proportional to the polarizability difference $\Delta\alpha = \alpha_{\parallel} - \alpha_{\perp}$ in the Rayleigh particle regime [24]. The rotational motion of the nanorod is typically described by the Langevin equation [24], $I\frac{d^2\beta}{dt^2} = N\sin^2\beta - \gamma\frac{d\beta}{dt}$, where I is the nanorod moment of inertia, β is the orientation angle, as defined before, $N = -\Delta\alpha E^2/4$ is the time-averaged torque amplitude, and γ is the angular drag coefficient from the Stokes law for rotation in a viscous medium. Clearly, in the waveguide channel induced by the soliton beam, the torque exerted by the soliton beam depends on the local intensity (as E^2 is the squared magnitude of the optical field). Results from our calculation of the torque are presented below.

We examine orientational ordering and associated optical birefringence by measuring the transmission of a probe beam with varying linear polarization through the soliton-induced waveguide channel. The optical property of the nanorods within the waveguide can be expressed as a refractive index ellipsoid analog to the birefringent crystal, with n_x and n_y being the two complex refractive indices along the principal axes [Fig. 1(e)]. In combination with the Malus law, the output power of the linearly polarized components of the probe beam along the principal axes can be written as

$$P_x = P_{\text{in}}\cos^2(\theta)\exp(-2\text{Im}(n_x)L_{\text{opt}}), \quad (3)$$

$$P_y = P_{\text{in}}\sin^2(\theta)\exp(-2\text{Im}(n_y)L_{\text{opt}}), \quad (4)$$

where $L_{\text{opt}} = 2\pi L/\lambda$ is phase that the light accumulates when passing through the cuvette (length L) without the medium. Im stands for the imaginary part. The total output power is $P_s = P_x + P_y$; thus, the transmission spectrum $T(\theta) = P_s/P_{\text{in}}$ will be simplified as

$$T = \exp(-2\text{Im}(n_x)L_{\text{opt}}) + \sin^2(\theta)[\exp(-2\text{Im}(n_y)L_{\text{opt}}) - \exp(-2\text{Im}(n_x)L_{\text{opt}})]. \quad (5)$$

Since the absorption of water is unlikely orientation dependent, in the transmission spectra, the global absorbance of water is neglected as we focus on distinguishing between optically induced nematic and isotropic phases of nanorods. The introduction of the soliton beam apparently enhances the optical transparency as shown in our transmission measurement. More interestingly, the refractive index experienced by the probe beam in the soliton-induced waveguide channel exhibits birefringence, producing polarization-dependent transmission of light according to Eq. (5). A modulation depth, $\eta = \exp(-2\text{Im}(n_y)L_{\text{opt}}) - \exp(-2\text{Im}(n_x)L_{\text{opt}})$, can be used to distinguish different phases. If no birefringence exists as in the isotropic phase, there will be no polarization-dependent modulation in the transmission measurement. (Recall that such a modulation vanishes in birefringent crystals for which there is no appreciable imaginary index.)

Our experimental setup is shown in Fig. 2(a). The gold nanorods used in our experiments have an average diameter of 50 nm and a length of 100 nm, which corresponds to a transverse surface plasmonic resonance (TSPR) at 520 nm, but an LSPR at 600 nm. A linearly polarized green soliton-forming beam at wavelength 532 nm (blue-detuned with respect to the LSPR) is focused to around 20 μm (FWHM) at the entrance surface of the suspension in a 40 mm long

cuvette by an achromatic lens with an 80 mm focal length. The output spatial transverse patterns are monitored by another achromatic lens ($f = 200$ mm), together with a CCD camera. At low input power, the green beam undergoes linear diffraction to a beam size of 1.4 mm, but as the power is increased to only 100 mW, a needle-like soliton channel is formed as seen from the side view image shown in Fig. 2(b). The zoom-in output pattern of the soliton beam shows a much reduced beam size [Fig. 2(c)]. These soliton results agree with our previous observations [17] but, in what follows, we focus on the orientational ordering effect induced by optical torques.

To measure the polarization transmission spectrum in order to facilitate the detection of the soliton-mediated phase transition described above, an IR probe beam (1064 nm) is launched into the soliton waveguide created by the 532 nm beam [17]. The IR beam is prepared to be circularly polarized, but then passes through a rotary polarizer, which allows the probe beam to have nearly constant power when its polarization direction is varied. The IR probe beam is set at a fairly low power (~10 mW), so it does not have any nonlinear self-action in the nanorod suspension. Typical guided output patterns of the weak IR beam with different polarization directions are shown in the bottom panels of Fig. 2, where Fig. 2(d) shows the natural linear diffraction of the probe beam when the soliton beam is absent, and Figs. 2(e)–2(h) show the guided output patterns when the soliton beam is turned on. The probe beam with different polarization orientations (0°, 30°, 60°, and 90°) is always guided in the soliton channel, as it experiences a higher refractive index along the soliton channel. The controlled polarization orientation facilitates the detection of the birefringence due to isotropic to nematic phase transition.

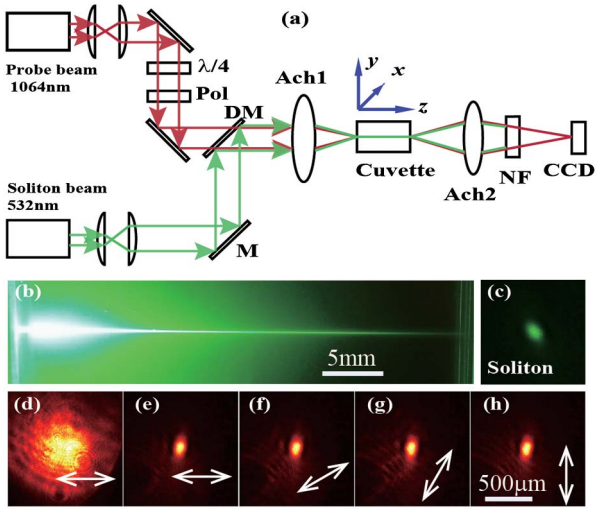

Fig. 2. (a) Schematic diagram of the experimental setup for soliton-mediated phase transition. The soliton-forming beam (532 nm) is collimated to 5 mm in diameter and then focused by an achromatic lens (Ach1) onto the input facet of the cuvette containing nanosuspension. A probe beam (1064 nm) at low power is sent through a dichroic mirror (DM), propagating collinearly with the green beam, and its polarization is regulated by a quarter-waveplate and a polarizer. The output intensity patterns of the IR beam are taken by a CCD camera, together with another achromatic lens (Ach2) and a notch filter (NF). (b), (c) Side view image of the green soliton beam and its zoom-in self-trapped transverse pattern. (d)–(h) Linear diffraction (d) and guided output of the probe beam (e–h) with its polarization angle θ at 0°, 30°, 60° and 90°.

This is done simply by measuring the transmitted power with a power meter placed in the output beam path after the green soliton beam is blocked by a notch filter.

Figure 3 shows the typical measured polarization transmission spectrum. For these results, the input power for both the soliton beam and the probe is fixed, and the only variable is the input polarization of the probe beam. The transmission (normalized to input power) is strongly modulated when the soliton beam is on, but remains fairly flat when the soliton beam is off. These results are in agreement with the prediction from Eq. (5). If we vary the input power of the soliton beam, the modulation depth becomes appreciable only when strong nonlinear self-trapping is achieved at high power levels around 100 mW, indicating that orientational ordering and resulting birefringence arise from the action of the soliton beam. For direct comparison, we also plot in Fig. 3 results obtained from gold nanosphere suspensions. The measured data points are fitted with the same sinusoidal model for both the on and off cases of the soliton beam, and it is found that the amplitude of modulation increased about 10 times from the off-to-on transition for the nanorods but, for nanospheres, the modulation (mainly due to experimental noise) kept in the level, since n_x and n_y are the same for nanospheres.

To have a quantitative understanding of the alignment process of nanorods under the action of a laser beam, we perform finite element calculations of the force and torque acting on a single nanorod. Shown in Fig. 4(a) is the torque exerted on a nanorod placed at the focus of the laser beam as a function of the orientation angle β, as defined in Fig. 1(b). The torque along the z-direction is much larger than that in the transverse directions, and changes its direction from counter-clockwise to clockwise when β increases over 90°. This clearly indicates that a nanorod tends to align its long axis perpendicular to the soliton beam polarization. Our calculations show that this alignment process still occurs when the nanorod is placed away from the beam focus along the lateral direction [Figs. 4(b) and 4(c)]. Experimentally, we also estimated the real part of the birefringence by sending a 45° linearly polarized beam into the nanorod suspension and measuring the output power after a polarization

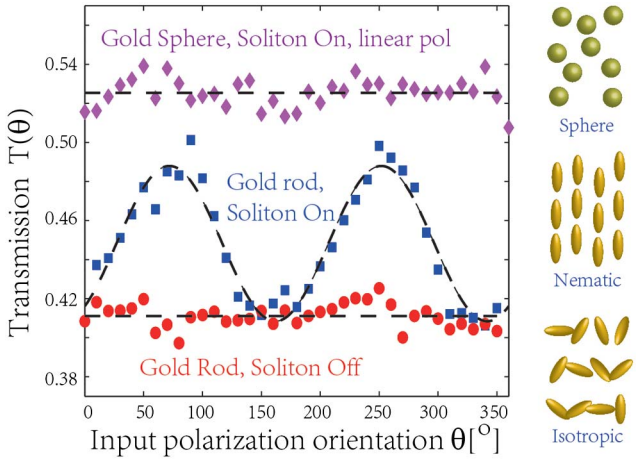

Fig. 3. Polarization transmission spectrum of the probe beam measured when the soliton beam is turned on (blue squares) and off (red dots) in a gold nanorod suspension, indicating orientational ordering from isotropic phase to nematic phase by the action of the soliton beam. The spectrum from a gold nanosphere suspension shows no appreciable modulation even with the soliton beam on (magenta diamonds).

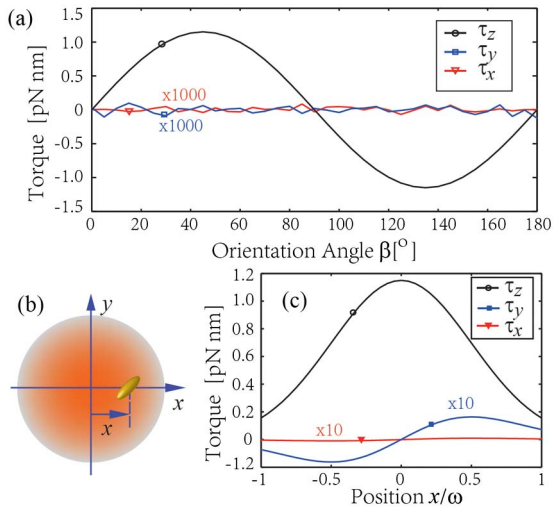

Fig. 4. (a) Calculated torque exerted by the soliton beam on a single gold nanorod at the beam center with different orientations. Note that torques in the x and y directions are magnified by a factor of 1000 for easy comparison. (b) Schematic of the position and orientation of a single nanorod located off the beam center and (c) the torque exerted on the nanorod as a function of the displacement x normalized by the beam waist ω from the beam center (the orientation of the rod is fixed). The torques along the x and y directions are magnified by a factor of 10.

analyzer. The measured phase shift between two orthogonal polarization components is about 1°, indicating the birefringence in nanorod suspensions is quite small.

To see if this alignment process is affected by the polarization of the soliton beam, we perform similar polarization transmission measurement in the soliton-induced waveguide, but with the soliton beam being circularly polarized. Figures 5(a) and 5(b) show the output transverse intensity patterns of linear diffraction and soliton formation of the circularly polarized green beam. As shown in Figs. 5(c) and 5(d), the IR probe beam is also guided by the soliton-induced waveguide channel. The measured polarization spectrum is shown in Fig. 5(e), which displays no appreciable difference between the cases when the soliton beam is on and off. This suggests that the circularly polarized soliton beam does not induce orientational ordering of the nanorods.

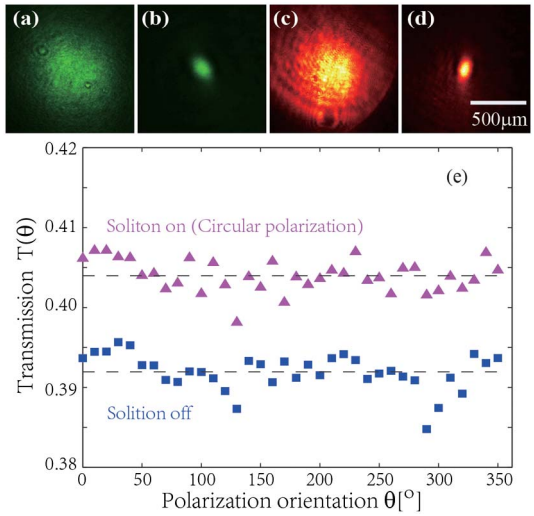

Fig. 5. Transverse output intensity patterns of a circularly polarized green beam showing (a) linear diffraction at low power and (b) nonlinear self-trapping at high power. (c), (d) Corresponding output patterns of the IR probe beam when the soliton beam is off and on, respectively. (e) Polarization transmission spectra show no significant difference when the soliton beam is turned on or off provided it is circularly polarized.

In conclusion, we have demonstrated soliton-mediated orientational ordering and birefringence in nonlinear gold nanorod suspensions. The orientation of the nanorods is disordered in a natural suspension, as driven by Brownian motion. Within the soliton-induced waveguide channel, however, the rotational fluctuation of the rods is suppressed, and the rods are aligned due to the optical torque resulting from the soliton beam. The concept of soliton-mediated ordering may be applied in other nonlinear colloidal and optofluidic systems, and may find applications in manipulation of light-matter interaction through plasmonic coupling.

Funding. National Science Foundation (NSF) (PHY-1404510); Army Research Office (ARO) (W911NF-15-1-0413, W911NF-16-1-0503); National Institutes of Health (NIH) (1R15GM112117-01).

REFERENCES

1. A. Jonáš and P. Zemánek, Electrophoresis **29**, 4813 (2008).
2. X. Huang, I. H. El-Sayed, W. Qian, and M. A. El-Sayed, J. Am. Chem. Soc. **128**, 2115 (2006).
3. W.-S. Chang, J. W. Ha, L. S. Slaughter, and S. Link, Proc. Natl. Acad. Sci. USA **107**, 2781 (2010).
4. S. Fardad, A. Salandrino, M. Heinrich, P. Zhang, Z. Chen, and D. N. Christodoulides, Nano Lett. **14**, 2498 (2014).
5. M. E. J. Friese, T. A. Nieminen, N. R. Heckenberg, and H. Rubinsztein-Dunlop, Nature **394**, 348 (1998).
6. A. La Porta and M. D. Wang, Phys. Rev. Lett. **92**, 190801 (2004).
7. A. Lehmuskero, P. Johansson, H. Rubinsztein-Dunlop, L. Tong, and M. Käll, ACS Nano **9**, 3453 (2015).
8. Y. Tanaka, H. Yoshikawa, T. Itoh, and M. Ishikawa, Opt. Express **17**, 18760 (2009).
9. M. Pelton, M. Liu, H. Y. Kim, G. Smith, P. Guyot-Sionnest, and N. F. Scherer, Opt. Lett. **31**, 2075 (2006).
10. C. Selhuber-Unkel, I. Zins, O. Schubert, C. Sönnichsen, and L. B. Oddershede, Nano Lett. **8**, 2998 (2008).
11. P. V. Ruijgrok, N. R. Verhart, P. Zijlstra, A. L. Tchebotareva, and M. Orrit, Phys. Rev. Lett. **107**, 037401 (2011).
12. J.-W. Liaw, Y.-S. Chen, and M.-K. Kuo, Appl. Phys. A **122**, 182 (2016).
13. J. Do, M. Fedoruk, F. Jäckel, and J. Feldmann, Nano Lett. **13**, 4164 (2013).
14. J. Trojek, L. Chvátal, and P. Zemánek, J. Opt. Soc. Am. A **29**, 1224 (2012).
15. K. Wang, S.-M. Jin, J. Xu, R. Liang, K. Shezad, Z. Xue, X. Xie, E. Lee, and J. Zhu, ACS Nano **10**, 4954 (2016).
16. Q. Liu, Y. Cui, D. Gardner, X. Li, S. He, and I. I. Smalyukh, Nano Lett. **10**, 1347 (2010).
17. T. S. Kelly, Y.-X. Ren, A. Samadi, A. Bezryadina, D. Christodoulides, and Z. Chen, Opt. Lett. **41**, 3817 (2016).
18. C. Conti and E. DelRe, Phys. Rev. Lett. **105**, 118301 (2010).
19. Y. Lamhot, A. Barak, O. Peleg, and M. Segev, Phys. Rev. Lett. **105**, 163906 (2010).
20. A. Piccardi, U. Bortolozzo, S. Residori, and G. Assanto, Opt. Lett. **34**, 737 (2009).
21. C. F. Bohren and D. R. Huffman, *Absorption and Scattering of Light by Small Particles* (Wiley-VCH, 2007), pp. 130–157.
22. R. El-Ganainy, D. N. Christodoulides, C. Rotschild, and M. Segev, Opt. Express **15**, 10207 (2007).
23. W. Man, S. Fardad, Z. Zhang, J. Prakash, M. Lau, P. Zhang, M. Heinrich, D. N. Christodoulides, and Z. Chen, Phys. Rev. Lett. **111**, 218302 (2013).
24. W. A. Shelton, K. D. Bonin, and T. G. Walker, Phys. Rev. E **71**, 036204 (2005).